AIAA SciTech Forum
6-10 January 2020, Orlando, FL
AIAA Scitech 2020 Forum

10.2514/6.2020-0045



# Study of Mach Number Effect for 3D Co-Flow Jet Wings at Cruise Conditions

Yang Wang * Gecheng Zha †
Dept. of Mechanical and Aerospace Engineering
University of Miami, Coral Gables, Florida 33124
E-mail: gzha@miami.edu



**Abstract**

This paper numerically studies the Mach number effect on cruise performance of 3D Co-Flow Jet (CFJ) wings at freestream Mach number of 0.15, 0.30, 0.35, 0.40, 0.46 and 0.50. The non-swept wing with three aspect ratios ($AR$) of 5, 10 and 20 based on CFJ-NACA-6421 airfoil are investigated. The numerical simulations employ the intensively validated in house FASIP CFD code, which utilizes a 3D RANS solver with Spalart-Allmaras (S-A) turbulence model, 3rd order WENO scheme for the inviscid fluxes, and 2nd order central differencing for the viscous terms. Similar to the previous 2D study, the 3D lift coefficient is increased with the Mach number due to compressibility effect. However, the overall aerodynamic efficiency and productivity are substantially dropped from 2D to 3D due to increased induced drag and the CFJ power coefficient. The penalty is further increased with the decreased aspect ratio. Compared with the baseline 3D wing with NACA-6421 airfoil at the same aspect ratio, the cruise lift coefficient is increased on the average by about 30% for $AR$ of 5 and 60% for $AR$ of 20. For the $AR$ of 20, the pure aerodynamic lift to drag ratio $C_L/C_D$ is also increased by about 30%. Considering the CFJ pumping power consumption, the equivalent aerodynamic efficiency $(C_L/C_D)_c$ is about the same as the baseline wing. The productivity efficiency $(C_L^2/C_D)_c$ are increased by about 30% due to the increased lift coefficient. For $AR$ of 5, no efficiency advantage is obtained even though the high cruise lift coefficient remains. The study indicates that the CFJ wing with a thick airfoil is advantageous for cruise at subsonic speed up to Mach number of 0.50, in particular for high aspect ratio wing.

## Nomenclature

| | |
|---|---|
| $CFJ$ | Co-flow jet |
| $AoA$ | Angle of attack |
| $LE$ | Leading Edge |
| $TE$ | Trailing Edge |
| $S$ | Planform area |
| $c$ | Airfoil chord |
| $U$ | Flow velocity |
| $q$ | Dynamic pressure $0.5\,\rho\,U^2$ |
| $p$ | Static pressure |
| $\eta$ | Pump efficiency |
| $\rho$ | Air density |

* Graduate Student
† Professor, AIAA associate Fellow

| | |
|---|---|
| $\dot{m}$ | Mass flow |
| $M$ | Mach number |
| $\omega$ | Pitching Moment |
| $P$ | Pumping power |
| $\infty$ | Free stream conditions |
| $_j$ | Jet conditions |
| $C_L$ | Lift coefficient $L/(q_\infty S)$ |
| $C_D$ | Drag coefficient $D/(q_\infty S)$ |
| $C_M$ | Moment coefficient |
| $C_\mu$ | Jet momentum coef. $\dot{m}_j U_j/(q_\infty S)$ |
| $(C_L/C_D)_c$ | CFJ airfoil corrected aerodynamic efficiency $L/(D + P/V_\infty)$ |
| $(C_L^2/C_D)_c$ | CFJ airfoil productivity efficiency $C_L^2/(C_D + P/V_\infty)$ |
| $Pc$ | Power coefficient $L/(q_\infty S V_\infty)$ |
| $PR$ | Total Pressure ratio of the CFJ pump |
| $M_{is}$ | Isentropic Mach Number |
| $M_\infty$ | Freestream Mach Number |
| $P_{tinj}$ | Total injection pressure |
| $P_{tsuc}$ | Total suction pressure |
| $V_{inj}/V_\infty$ | Normalized injection velocity |



# 1 Introduction

High cruise efficiency is crucial to minimize the energy consumption of airliners. This is particular important for electric aircraft development to extend range and increase payload with the current limited battery energy density. However, increasing aircraft aerodynamic efficiency at cruise condition is very challenging because the flow condition is usually very benign at a low angle of attack. Most of the efforts to increase cruise efficiency in the past few decades are focused on 3D combination, including winglet, wing body combination, flying wing, boundary layer ingestion with integrated propulsion system and fuselage, distributed propulsion, etc. Few efforts are focused on improving the airfoil performance at cruise condition since they are considered mature with little room to improve.

Recently, the Co-Flow Jet (CFJ) flow control airfoil developed [1, 2, 3, 4, 5, 6, 7, 8, 9, 10, 11, 12] provides a promising concept to improve the cruise efficiency. In a CFJ airfoil, an injection slot near the leading edge (LE) and a suction slot near the trailing edge (TE) on the airfoil suction surface are created. As shown in Fig. 1, a small amount of mass flow is drawn into the suction duct, pressurized and energized by the micro compressor, and then injected near the LE tangentially to the main flow via an injection duct. The whole process does not add any mass flow to the system and hence is a zero-net-mass-flux(ZNMF) flow control. The CFJ airfoil is demonstrated to achieve radical lift augmentation, stall margin increase, drag reduction and increased nose-down moment for stationary and pitching airfoils.

The CFJ airfoil has a unique low energy expenditure mechanism, because the jet gets injected at the leading edge peak suction location, where the main flow pressure is the lowest and makes it easy to inject the flow, and it gets sucked at the trailing edge, where the main flow pressure is the highest and makes it easy to draw the flow. The low energy expenditure is a key factor enabling the CFJ airfoil to achieve high cruise efficiency [13] at low $AoA$ when the flow is benign.

Since aircraft operate at different cruise speeds, a question that needs to ask is how freestream Mach number affects the CFJ wings' aerodynamic performance and efficiency. Wang and Zha studied the 2D CFJ airfoil cruise performance at different Mach numbers [14]. Their study indicates that the 2D CFJ airfoil is able to significantly increase the cruise lift coefficient and aerodynamic efficiency. However, a 3D wing with finite wing span will introduce the induced drag,the higher the lift, the greater the induced drag. In [15], the 3D CFJ wing effect due to aspect ratio is studied at a fixed Mach number of 0.15. The cruise lift coefficient is increased substantially. The aerodynamic efficiency and productivity efficiency are also increased significantly at high aspect ratio. The efficiency advantage diminishes when the aspect ratio is decreased. No study is done to understand the 3D CFJ wing with variation of the Mach number.

The purpose of this paper is to extend the previous studies [14, 15] to 3D CFJ wings with varying Mach number and aspect ratio. The study indicates that the 2D CFJ aerodynamic efficiency improvement is largely offset by the increased induced drag due to the enhanced cruise lift coefficient. However, the productivity efficiency is still largely increased due to the augmented cruise lift coefficient.



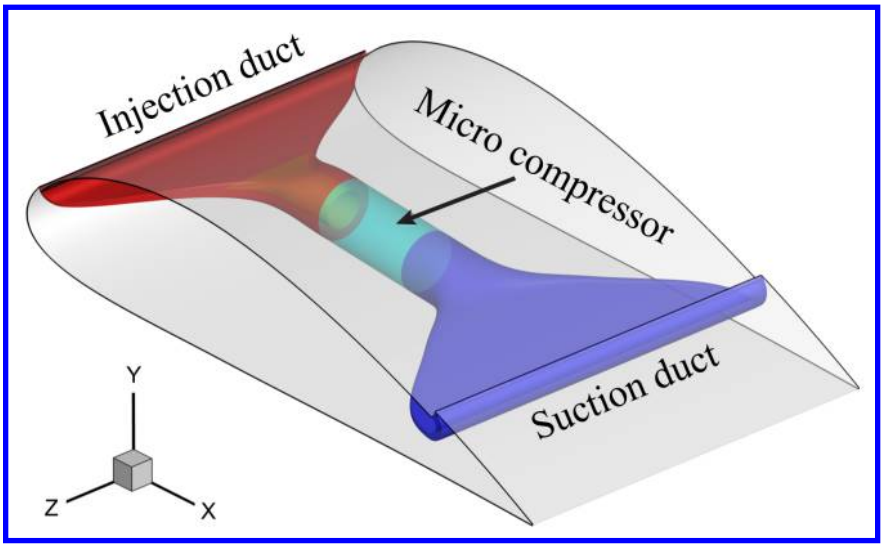


Figure 1: Schematic plot of a typical CFJ airfoil.

## 2 Co-Flow Jet Parameters

### 2.1 Lift and Drag Calculation

The momentum and pressure at the injection and suction slots produce a reactionary force, which is automatically measured by the force balance in wind tunnel testing. However, for CFD simulation, the full reactionary force needs to be included. Using control volume analysis as shown in Fig. 2, the reactionary force can be calculated using the flow parameters at the injection and suction slot opening surfaces. Zha et al. [2] give the following formulations to calculate the lift and drag due to the jet reactionary force for a CFJ airfoil. By considering the effects of injection and suction jets on the CFJ airfoil, the expressions for these reactionary forces are given as :

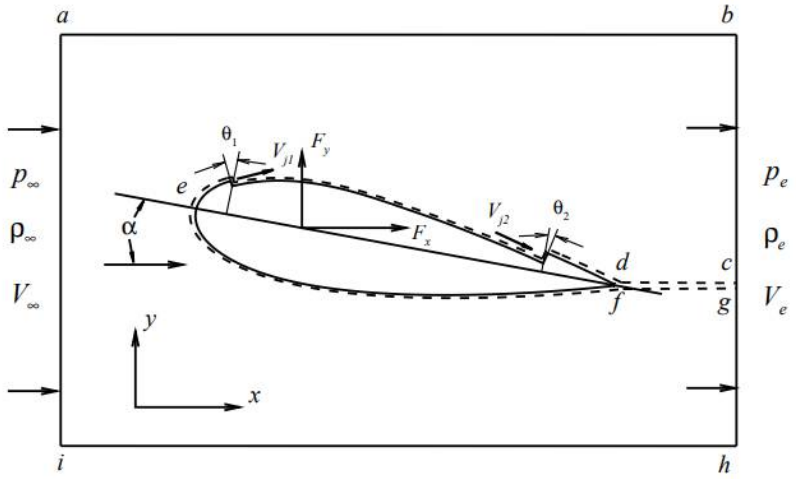


Figure 2: The control volume for a CFJ airfoil.

$$F_{x_{cfj}} = (\dot{m}_j V_{j1} + p_{j1} A_{j1}) * cos(\theta_1 - \alpha) - (\dot{m}_j V_{j2} + p_{j2} A_{j2}) * cos(\theta_2 + \alpha) \tag{1}$$

$$F_{y_{cfj}} = (\dot{m}_{j1} V_{j1} + p_{j1} A_{j1}) * sin(\theta_1 - \alpha) + (\dot{m}_{j2} V_{j2} + p_{j2} A_{j2}) * sin(\theta_2 + \alpha) \tag{2}$$

where the subscripts 1 and 2 stand for the injection and suction respectively, and $\theta_1$ and $\theta_2$ are the angles between the injection and suction slot's surface and a line normal to the airfoil chord. $\alpha$ is the angle of attack.

The total lift and drag on the airfoil can then be expressed as:

$$D = R'_x - F_{x_{cfj}} \tag{3}$$

$$L = R'_y - F_{y_{cfj}} \tag{4}$$

where $R'_x$ and $R'_y$ are the surface integral of pressure and shear stress in $x$ (drag) and $y$ (lift) direction excluding the internal ducts of injection and suction. For CFJ wing simulations, the total lift and drag are calculated by integrating Eq. (3) and Eq. (4) in the spanwise direction.

## 2.2 Jet Momentum Coefficient

The jet momentum coefficient $C_\mu$ is a parameter used to quantify the jet intensity. It is defined as:

$$C_\mu = \frac{\dot{m} V_j}{\frac{1}{2} \rho_\infty {V_\infty}^2 S} \tag{5}$$

where $\dot{m}$ is the injection mass flow, $V_j$ is the mass-averaged injection velocity, $\rho_\infty$ and $V_\infty$ denote the free stream density and velocity, and S is the planform area.

## 2.3 Power Coefficient

CFJ is implemented by mounting a pumping system inside the wing that withdraws air from the suction slot and blows it into the injection slot. The power consumption is determined by the jet mass flow and total enthalpy change as the following:

$$P = \dot{m}(H_{t1} - H_{t2}) \tag{6}$$

where $H_{t1}$ and $H_{t2}$ are the mass-averaged total enthalpy in the injection cavity and suction cavity respectively, $P$ is the Power required by the pump and $\dot{m}$ the jet mass flow rate. Introducing $P_{t1}$ and $P_{t2}$ the mass-averaged total pressure in the injection and suction cavity respectively, the pump efficiency $\eta$, and the total pressure ratio of the pump $\Gamma = \frac{P_{t1}}{P_{t2}}$, the power consumption is expressed as:

$$P = \frac{\dot{m} C_p T_{t2}}{\eta}(\Gamma^{\frac{\gamma-1}{\gamma}} - 1) \tag{7}$$

where $\gamma$ is the specific heat ratio equal to 1.4 for air. The power coefficient is expressed as:

$$P_c = \frac{P}{\frac{1}{2}\rho_\infty V_\infty^3 S} \tag{8}$$

## 2.4 Corrected Aerodynamic Efficiency

The conventional wing aerodynamic efficiency is defined as:

$$\frac{L}{D} \tag{9}$$

For the CFJ wing, the ratio above still represents the pure aerodynamic relationship between lift and drag. However since CFJ active flow control consumes energy, the ratio above is modified to take into account the energy consumption of the pump. The formulation of the corrected aerodynamic efficiency for CFJ wings is:

$$(\frac{L}{D})_c = \frac{C_L}{C_D + P_c} \tag{10}$$

where $V_\infty$ is the free stream velocity, $P$ is the pumping power, and $L$ and $D$ are the lift and drag generated by the CFJ wing. The formulation above converts the power consumed by the CFJ into a force $\frac{P}{V_\infty}$ which is added to the aerodynamic drag D. If the pumping power is set to 0, this formulation returns to the aerodynamic efficiency of a conventional wing.

## 2.5 Aircraft Productivity

To compare aircraft that have the same ratio of initial weight to final weight with the same engine fuel consumption or battery energy density, the productivity efficiency $C_L^2/C_D$ is introduced to measure the productivity of an airplane represented by its range multiplied by its weight [16].

The productivity efficiency $C_L^2/C_D = C_L(C_L/C_D)$ is a more comprehensive parameter than the conventional aerodynamic efficiency $C_L/C_D$ to measure the merit of an airplane aerodynamic design for cruise performance. The former includes not only the information of $C_L/C_D$, but also the information of the aircraft weight $C_L$. For example, for two airplane designs having the same $C_L/C_D$ with one $C_L$ twice larger than the other, if the wing sizes are the same, one airplane will be able to carry twice more weight than the other with productivity and wing loading increased by 100%. Such a large difference is not reflected by $C_L/C_D$, but very well reflected by $C_L^2/C_D$.

The definition of $C_L/C_D$ in general is a suitable measure of merit for conventional aircraft design. This is because at a certain Mach number regime, the maximum $C_L/C_D$ is usually achieved at low angle of attack within the drag bucket and is more or less the same for different airfoil designs. In other words, for the same optimum $C_L/C_D$, the $C_L$ is about the same. A typical $C_L$ for subsonic airfoil is about 0.4 and for transonic airfoil is about 0.7.

For CFJ airfoil, the minimum CFJ pumping power occurs at a fairly high $AoA$ [7, 17]. With the augmentation of CFJ, the subsonic cruise lift coefficient of a CFJ airfoil is typically 2 to 3 times higher than the conventional airfoil with about the same $(C_L/C_D)_c$ [12]. Such a high lift coefficient is unattainable for conventional airfoil since they would be either stalled or near stalled with very high drag. Hence for CFJ aircraft design, the productivity efficiency $C_L^2/C_D = C_L(C_L/C_D)$ is more informative to be used to reflect the aerodynamic performance. The corrected productivity efficiency for CFJ airfoils is $(C_L^2/C_D)_c = C_L^2/(C_D + P_c)$.



# 3 Numerical Algorithms

## 3.1 CFD Simulation Setup

The in house FASIP (Flow-Acoustics-Structure Interaction Package) CFD code is used to conduct the numerical simulation. The 3D Reynolds Averaged Navier-Stokes (RANS) equations with one-equation Spalart-Allmaras [18] turbulence model is used. A 3rd order WENO scheme for the inviscid flux [19, 20, 21, 22, 23, 24] and a 2nd order central differencing for the viscous terms [19, 23] are employed to discretize the Navier-Stokes equations. The low diffusion E-CUSP scheme used as the approximate Riemann solver suggested by Zha et al [20] is utilized with the WENO scheme to evaluate the inviscid fluxes. Implicit time marching method using Gauss-Seidel line relaxation is used to achieve a fast convergence rate [25]. Parallel computing is implemented to save wall clock simulation time [26].

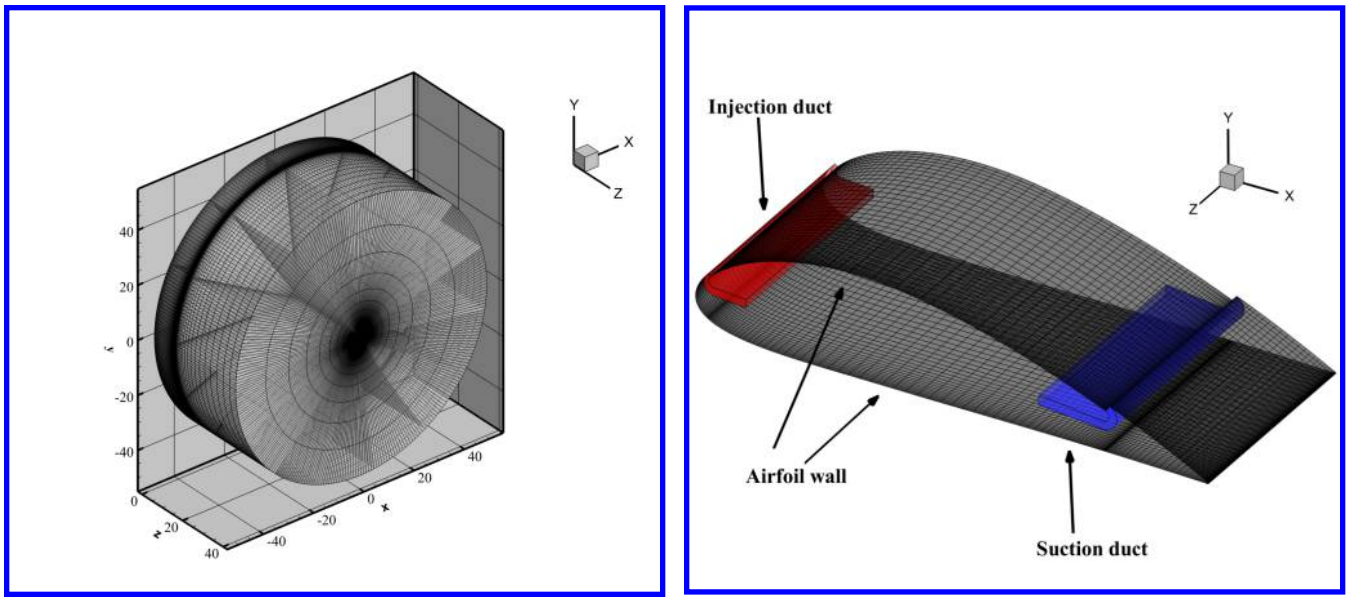


Figure 3: Computational mesh used in the current work.

### 3.2 Boundary Conditions

The 3rd order accuracy no slip condition is enforced on the solid surface with the wall treatment suggested in [27] to achieve the flux conservation on the wall. The computational mesh is shown in Fig. 3 with O-mesh topology and the radial farfield boundary located at 20 chord radius. The spanwise farfield is located at 20 chord away from the wing tip. The ducts geometries are predetermined based on our previous 2D designs [14]. Total pressure, total temperature and flow angles are specified at the injection duct inlet, as well as the upstream portion of the far field. Constant static pressure is applied at the suction duct outlet as well as the downstream portion of the far field. Symmetry boundary conditions are applied at the root of the wing, whereas the wing tip flow is resolved by a mesh block. The cross-section faces of the CFJ ducts are meshed using "H" topology while the domains around the airfoil are meshed using "O" topology. The total mesh size is 3.918 millions points, split into 111 blocks for the parallel computation. The first grid point on the wing surface is placed at $y^+ \approx 1$. This mesh size is the same as the mesh size used in the study of Wang and Zha [15], for which the mesh refinement is verified for mesh independence.

## 4 Results and Discussion

### 4.1 CFJ Wing Geometry Parameters

The detailed parameters of CFJ airfoil used to create the 3D CFJ wing are presented by the injection and suction slot size normalized by airfoil chord length (C). The CFJ6421-SST150-SUC247-INJ117 airfoil designed in [14, 15] is optimized by enlarging the injection and suction size based on the CFJ airfoil from [12]. The CFJ6421-SST150-SUC247-INJ117 wing has a injection slot size of 1.17%C and suction slot size of 2.47%C. The suction surface translation (SST) is 1.50%C.

Table. 1 lists all the freestream conditions studied with the Mach number varying from 0.15 to 0.50 at the

aspect ratio of 5, 10, and 20. Since the focus is on the cruise performance, the $AoA$ is fixed at 5° and the $C_\mu$ is fixed at 0.03. The $AoA$ of 5° and $C_\mu$ of 0.03 give the optimum aerodynamic efficiency for all the Mach numbers except for 0.50, for which the optimum condition is at $AoA$ of 2° and $C_\mu$ of 0.01 due to avoiding the transonic shock wave.

Table 1: Simulation cases

| $M_\infty$ | $AoA$ | $C_\mu$ | AR |
|---|---|---|---|
| 0.15 | 0° - 14° | 0.03 | 5, 10, 20 |
| 0.30 | 0° - 14° | 0.03 | 5, 10, 20 |
| 0.35 | 0° - 14° | 0.03 | 5, 10, 20 |
| 0.40 | 0° - 14° | 0.03 | 5, 10, 20 |
| 0.46 | 0° - 14° | 0.03 | 5, 10, 20 |
| 0.50 | 0° - 14° | 0.01 | 5, 10, 20 |



### 4.2 3D CFJ Wing at Different $M_\infty$ and $AoA$

This section discusses the performance of 3D CFJ Wing and 2D CFJ Airfoil at Different $M_\infty$ and $AoA$. As we can seen from these tables, the $AoA$ of 5° and 6° always give the best CFJ corrected aerodynamic efficiency. Thus, the analysis of 3D CFJ wing performance is based on the $AoA$ of 5°. The results of $M_\infty$ of 0.15, 0.35, and 0.40 are not listed below to save space. The $M_\infty$ of 0.30 has higher compressibility than that at $M_\infty$ of 0.15, but is still far from the sonic speed. At $M_\infty$ of 0.46, the critical Mach number for the airfoil, the CFJ corrected aerodynamic efficiency is still very good since no shock appears in the flow filed. But when the $M_\infty$ is increased to 0.50, the flow becomes transonic and the optimum aerodynamic efficiency occurs at a lower $AoA$ of 2° and $C_\mu$ of 0.01. Thus, these three representative Mach number (0.30, 0.46, and 0.50) are chosen to present more detailed results.

Table. 2 and Table. 3 show the performance of 3D CFJ wings at $M_\infty$ of 0.30 and $C_\mu$ of 0.03 at different $AoA$.

Table 2: Performance at $M_\infty$ 0.30 for the 3D CFJ Wing at $AR$ 20 and different $AoA$ and $C_\mu$ of 0.03.

| $AoA$ | $C_L$ | $C_L/C_D$ | $(C_L/C_D)_c$ | $({C_L}^2/C_D)_c$ | $P_c$ | $PR$ | $P_{tinj}$ | $\dot{m}/Span$ | $V_{inj}$ |
|---|---|---|---|---|---|---|---|---|---|
| 0° | 0.724 | 46.477 | 23.973 | 17.346 | 0.015 | 1.101 | 8.747 | 0.013 | 1.133 |
| 2° | 0.936 | 43.932 | 27.479 | 25.717 | 0.013 | 1.091 | 8.591 | 0.013 | 1.145 |
| 5° | 1.237 | 36.558 | 28.741 | 35.545 | 0.009 | 1.074 | 8.327 | 0.013 | 1.165 |
| 6° | 1.324 | 34.079 | 28.198 | 37.344 | 0.008 | 1.067 | 8.230 | 0.013 | 1.173 |
| 10° | 1.156 | 11.573 | 10.386 | 12.003 | 0.011 | 1.094 | 8.152 | 0.013 | 1.169 |
| 14° | 0.984 | 6.332 | 5.686 | 5.595 | 0.018 | 1.132 | 8.146 | 0.013 | 1.176 |

Table 3: Performance at $M_\infty$ 0.30 for the 3D CFJ Wing at $AR$ 10 and different $AoA$ and $C_\mu$ of 0.03.

| $AoA$ | $C_L$ | $C_L/C_D$ | $(C_L/C_D)_c$ | $({C_L}^2/C_D)_c$ | $P_c$ | $PR$ | $P_{tinj}$ | $\dot{m}/Span$ | $V_{inj}$ |
|---|---|---|---|---|---|---|---|---|---|
| 0° | 0.646 | 30.658 | 17.891 | 11.556 | 0.015 | 1.071 | 8.779 | 0.013 | 1.131 |
| 2° | 0.835 | 27.763 | 19.237 | 16.064 | 0.013 | 1.064 | 8.639 | 0.013 | 1.140 |
| 5° | 1.110 | 23.085 | 19.016 | 21.117 | 0.010 | 1.050 | 8.386 | 0.013 | 1.158 |
| 6° | 1.196 | 21.632 | 18.503 | 22.123 | 0.009 | 1.045 | 8.305 | 0.013 | 1.165 |
| 10° | 1.430 | 16.310 | 15.431 | 22.074 | 0.005 | 1.025 | 7.966 | 0.013 | 1.188 |
| 14° | 0.984 | 6.115 | 5.611 | 5.519 | 0.014 | 1.072 | 8.081 | 0.013 | 1.170 |

Table. 4 and Table. 5 show the performance of 3D CFJ wings at $M_\infty$ of 0.46 and $C_\mu$ of 0.03 at different $AoA$.

Table 4: Performance at $M_\infty$ 0.46 for the 3D CFJ Wing at $AR$ 20 and different $AoA$ and $C_\mu$ of 0.03.

| $AoA$ | $C_L$ | $C_L/C_D$ | $(C_L/C_D)_c$ | $({C_L}^2/C_D)_c$ | $P_c$ | $PR$ | $P_{tinj}$ | $\dot{m}/Span$ | $V_{inj}$ |
|---|---|---|---|---|---|---|---|---|---|
| 0° | 0.800 | 47.593 | 25.031 | 20.030 | 0.015 | 1.168 | 4.245 | 0.014 | 1.120 |
| 2° | 1.036 | 43.477 | 27.539 | 28.532 | 0.014 | 1.156 | 4.095 | 0.013 | 1.144 |
| 5° | 1.316 | 36.179 | 27.501 | 36.179 | 0.011 | 1.196 | 3.842 | 0.013 | 1.186 |
| 6° | 1.479 | 33.050 | 26.842 | 39.688 | 0.010 | 1.122 | 3.741 | 0.013 | 1.208 |
| 10° | 1.238 | 11.807 | 10.474 | 12.964 | 0.013 | 1.164 | 3.658 | 0.012 | 1.213 |
| 14° | 1.033 | 6.626 | 5.866 | 6.059 | 0.020 | 1.258 | 3.549 | 0.012 | 1.233 |

Table 5: Performance at $M_\infty$ 0.46 for the 3D CFJ Wing at $AR$ 10 and different $AoA$ and $C_\mu$ of 0.03.

| $AoA$ | $C_L$ | $C_L/C_D$ | $(C_L/C_D)_c$ | $({C_L}^2/C_D)_c$ | $P_c$ | $PR$ | $P_{tinj}$ | $\dot{m}/Span$ | $V_{inj}$ |
|---|---|---|---|---|---|---|---|---|---|
| 0° | 0.705 | 30.522 | 18.362 | 12.950 | 0.015 | 1.170 | 4.276 | 0.014 | 1.109 |
| 2° | 0.913 | 26.979 | 19.013 | 17.356 | 0.014 | 1.159 | 4.155 | 0.013 | 1.133 |
| 5° | 1.223 | 21.931 | 18.132 | 22.168 | 0.012 | 1.135 | 3.913 | 0.013 | 1.173 |
| 6° | 1.314 | 20.652 | 17.542 | 23.053 | 0.011 | 1.131 | 3.847 | 0.013 | 1.187 |
| 10° | 1.590 | 15.853 | 14.689 | 23.351 | 0.008 | 1.097 | 3.521 | 0.012 | 1.244 |
| 14° | 1.026 | 6.162 | 5.562 | 5.706 | 0.018 | 1.226 | 3.603 | 0.012 | 1.221 |

Table. 6 and Table. 7 show the performance of 3D CFJ wings and 2D CFJ airfoil at $M_\infty$ of 0.50 and $C_\mu$ of 0.01 at different $AoA$. As the results show on previous 2D Mach number study [14], the best performance for $M_\infty$ of 0.50 is at $AoA$ of 2° instead of $AoA$ of 6°, and $C_\mu$ of 0.01 instead of 0.03. This is because the flow becomes transonic at $M_\infty$ of 0.50 with shock wave appearance. The same $AoA$ and $C_\mu$ from the 2D study are adopted for this 3D wing study.

Table 6: Performance at $M_\infty$ 0.50 for the 3D CFJ Wing at $AR$ 20 and different $AoA$ and $C_\mu$ of 0.01.

| $AoA$ | $C_L$ | $C_L/C_D$ | $(C_L/C_D)_c$ | $(C_L{}^2/C_D)_c$ | $P_c$ | $PR$ | $P_{tinj}$ | $\dot{m}/Span$ | $V_{inj}$ |
|---|---|---|---|---|---|---|---|---|---|
| 0° | 0.714 | 40.770 | 30.953 | 22.097 | 0.006 | 1.125 | 3.226 | 0.008 | 0.654 |
| 2° | 0.913 | 36.738 | 31.507 | 28.762 | 0.004 | 1.094 | 3.081 | 0.008 | 0.670 |
| 5° | 1.135 | 27.829 | 26.744 | 30.343 | 0.002 | 1.039 | 2.855 | 0.007 | 0.698 |
| 6° | 0.840 | 10.620 | 10.177 | 8.544 | 0.003 | 1.081 | 2.953 | 0.007 | 0.680 |
| 10° | 0.701 | 5.354 | 5.122 | 3.590 | 0.006 | 1.145 | 2.847 | 0.007 | 0.693 |
| 14° | 0.721 | 3.489 | 3.399 | 2.451 | 0.005 | 1.135 | 2.747 | 0.007 | 0.710 |

Table 7: Performance at $M_\infty$ 0.50 for the 3D CFJ Wing at $AR$ 10 and different $AoA$ and $C_\mu$ of 0.01.

| $AoA$ | $C_L$ | $C_L/C_D$ | $(C_L/C_D)_c$ | $(C_L{}^2/C_D)_c$ | $P_c$ | $PR$ | $P_{tinj}$ | $\dot{m}/Span$ | $V_{inj}$ |
|---|---|---|---|---|---|---|---|---|---|
| 0° | 0.622 | 27.617 | 22.043 | 13.706 | 0.006 | 1.128 | 3.264 | 0.008 | 0.649 |
| 2° | 0.803 | 24.816 | 21.812 | 17.512 | 0.004 | 1.101 | 3.136 | 0.008 | 0.663 |
| 5° | 1.025 | 19.828 | 19.030 | 19.507 | 0.002 | 1.050 | 2.928 | 0.007 | 0.688 |
| 6° | 0.796 | 9.852 | 9.550 | 7.599 | 0.003 | 1.059 | 2.983 | 0.007 | 0.675 |
| 10° | 0.688 | 5.238 | 5.051 | 3.477 | 0.005 | 1.117 | 2.869 | 0.007 | 0.688 |
| 14° | 0.703 | 3.456 | 3.376 | 2.373 | 0.005 | 1.118 | 2.765 | 0.007 | 0.704 |



### 4.3 3D CFJ Wing Cruise Performance at Different Mach Number

The cruise lift, drag and moment coefficients vs. $M_\infty$ for the 3D CFJ and baseline wing at different AR are shown in Fig. 4 with the 2D CFJ airfoil results [14]. As the $M_\infty$ increases, all the CFJ coefficient of lift, drag and nose down pitching moment also are increased due to the compressibility effect, whereas the baseline wing has all those coefficients fairly. As expected, the drag coefficient of the higher $AR$ is smaller than the lower $AR$ case due to decreased induced drag. The nose down moment $C_M$ is increased with the $C_L$.

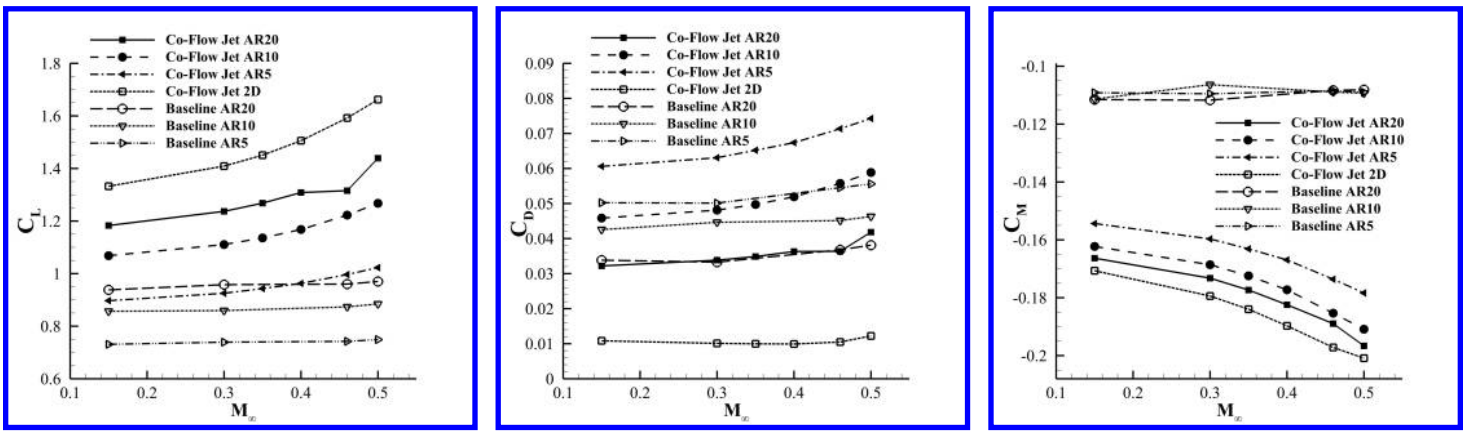


(a) (b) (c)

Figure 4: Lift, drag and moment coefficients for the 3D CFJ wings and 2D CFJ airfoil.

The $C_L/C_D$, $(C_L/C_D)_c$, $(C_L{}^2/C_D)_c$ at different Mach number are substantially lower than the 2D CFJ airfoil

due to the induced drag penalty as shown in Fig. 5. All the 3D results remain fairly constant with the Mach number, whereas the 2D aerodynamic efficiency and productivity efficiency are increased with the Mach number until it reaches Mach number of 0.50, which reaches the transonic regime with shock wave.

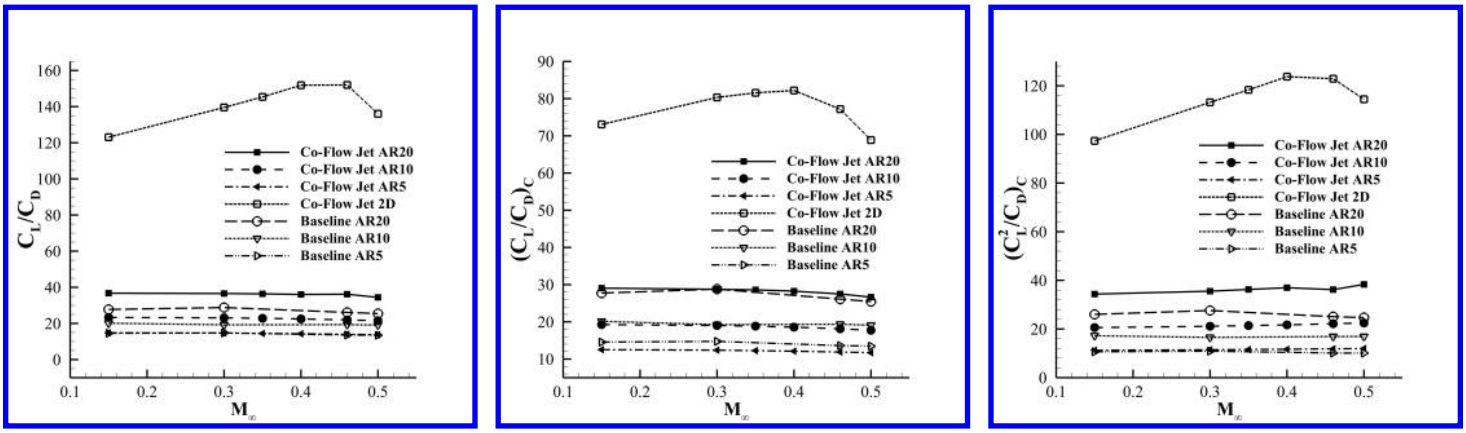


(a) (b) (c)

Figure 5: $C_L/C_D$, $(C_L/C_D)_c$, $(C_L{}^2/C_D)_c$ plots for the 3D CFJ wings and 2D CFJ airfoil.

Compared with the baseline 3D wing with NACA-6421 airfoil at the same aspect ratio, the cruise lift coefficient is increased on the average by about 30% for $AR$ of 5 and 60% for $AR$ of 20 as shown in Fig. 4. For the $AR$ of 20, the pure aerodynamic lift to drag ratio $C_L/C_D$ is also increased by about 30% as displayed in Fig. 5. Considering the CFJ pumping power consumption, the equivalent aerodynamic efficiency $C_L/C_{D_c}$ is about the same as the baseline wing. The productivity efficiency $C_L^2/C_{D_c}$ are increased by about 30% due to the increased lift coefficient. For $AR$ of 5, no efficiency advantage is obtained even though the high cruise lift coefficient remains.

CFJ makes the thick airfoil beneficial for the aircraft system by providing large lift coefficient and lighter structure weight. As shown in Fig. 4 and Fig. 5, the cruise lift coefficient of the CFJ wing at $AR$ of 20 reaches 1.45 at Mach 0.5 while keeping a $C_L/C_D$ of 28 similar to the baseline wing. Such a high lift coefficient for cruise is unachievable for conventional subsonic wing with a typical cruise lift coefficient of 0.5-0.7. At a $C_L$ of 1.45, the conventional wing will be either stalled or near being stalled. Since CFJ wing can tolerate very high angle of attack without being stalled, such a thick airfoil wing is thus very feasible and efficient for subsonic aircraft.

As shown in Fig. 6, the 3D CFJ wing power coefficient increases linearly with the Mach number until it is greater than Mach 0.46 with more increased rate due to approaching transonic regime.

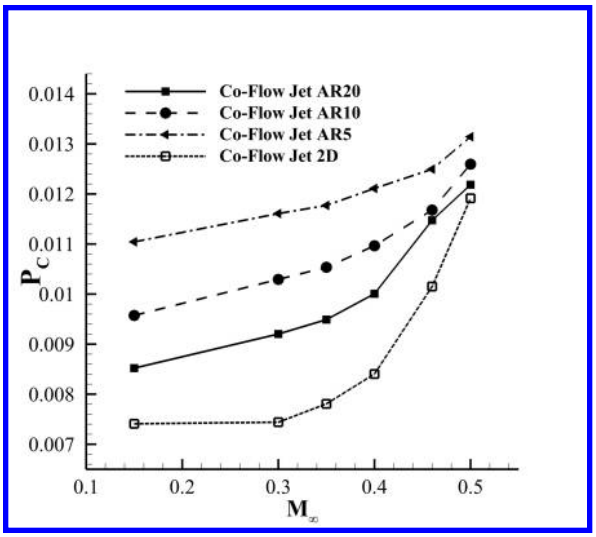


Figure 6: $P_c$ plot for the 3D CFJ wings and 2D CFJ airfoil.

Fig. 7 shows the Isentropic Mach number distribution of the wing section from root to tip at different span locations. Compared with the 2D case, the loading is substantially decreased as also reflected by the lift coefficient in Fig. 4 (a). At the outer span close to the wing tip, the loading is decreased due to wing tip vortices. Again, a higher aspect ratio always has a higher loading due to less effect of the tip vortex. The maximum Mach number is also shown in Fig. 11 and Fig. 12.

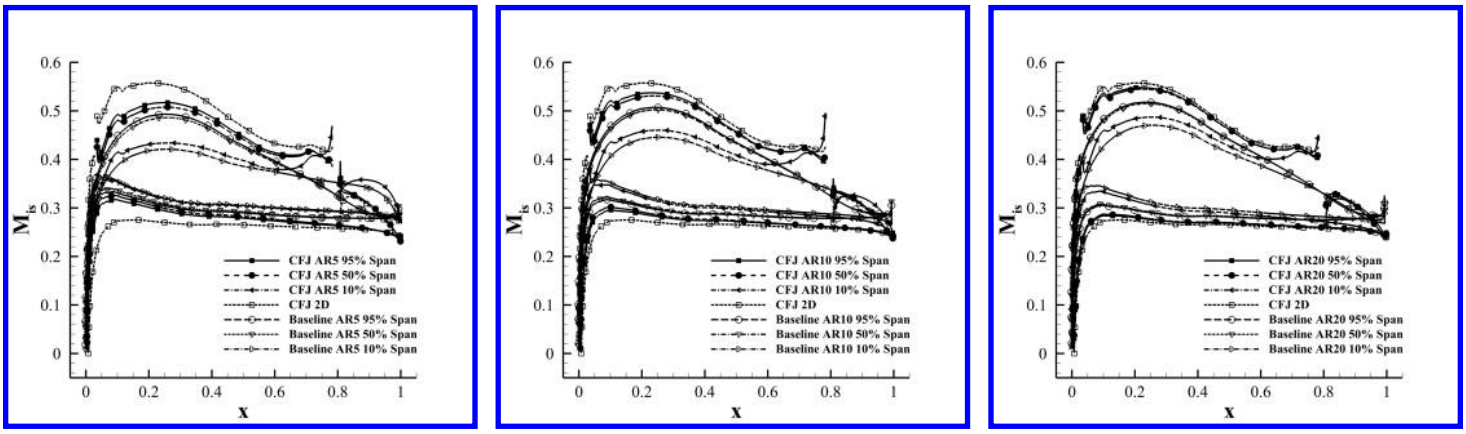


(a) AR 5 (b) AR 10 (c) AR 20

Figure 7: Isentropic Mach Number plots for the 3D CFJ wings and 2D CFJ airfoil at $M_\infty$ of 0.30, $C_\mu$ of 0.03, and $AoA$ of 5° with different $AR$.

Fig. 8 (a) and (b) are the normalized injection total pressure and the total pressure ratio between injection and suction. The pressure is normalized as:

$$\bar{p} = p/(\rho_\infty V_\infty^2) \tag{11}$$

Fig. 8 (a) indicates that to achieve the same injection momentum coefficient, the injection total pressure is decreased with the increasing Mach number. This is because the leading edge suction effect is greater and the

main flow pressure is lower in that region. Since the overall pressure level is lower with increased Mach number, the CFJ suction slot static pressure is also reduced. However, the important parameter determining the power consumption is the total pressure ratio between the injection and suction slot as shown in Fig. 8 (b). For cruise Mach number at 0.15 and $AoA$ of 5°, the total pressure ratio is at the level of 1.02. For Mach number of 0.3 and 0.46, it is increased to 1.08 and 1.2 respectively. For the cruise Mach number of 0.5 at $AoA$ of 5°, the total pressure ratio is about 1.24. The required CFJ total pressure ratio is increased with increasing Mach number due to the boundary layer suffering more loss at higher speed. It is the main reason that the power coefficient is increased with Mach number as shown in Fig. 6. For the same $C_\mu$, the total pressure ratio of the 3D cases vary little with aspect ratio and is also about the same as the 2D case.

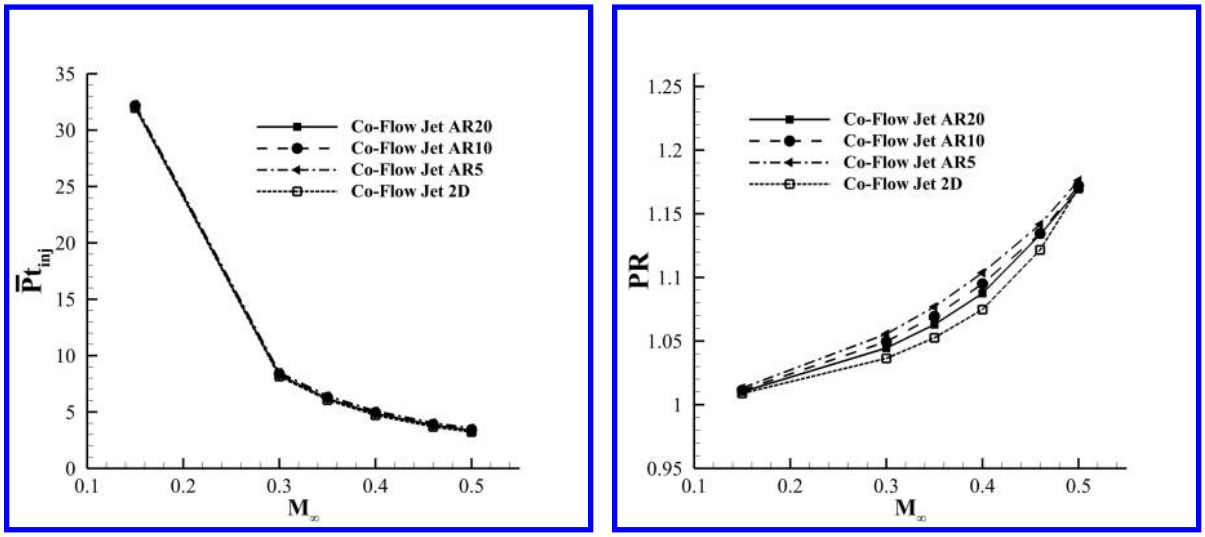


(a) (b)

Figure 8: Injection total pressure and the total pressure ratio between injection and suction plots for the 3D CFJ wings and 2D CFJ airfoil.

Fig. 9 (a) shows the normalized mass flow rate per unit span at injection, which shows that with decreased aspect ratio, the normalized mass flow rate per unit span is increased. This is the main reason that the power coefficient is increased with the decreased aspect ratio as shown in Fig. 6. Fig. 9 (b) shows the mass averaged injection jet speed normalized by the freestream speed. The normalized jet speed is increased with the Mach number from 1.14 at Mach 0.15 to 1.19 at Mach 0.50. Overall, the jet speed ratio is low and is beneficial for the low power required at cruise (Fig. 6)and the high efficiency shown in Fig. 5. Also, the normalized injection jet speed is a little lower than that at 2D and the lower aspect ratio wing has a lower injection speed ratio.

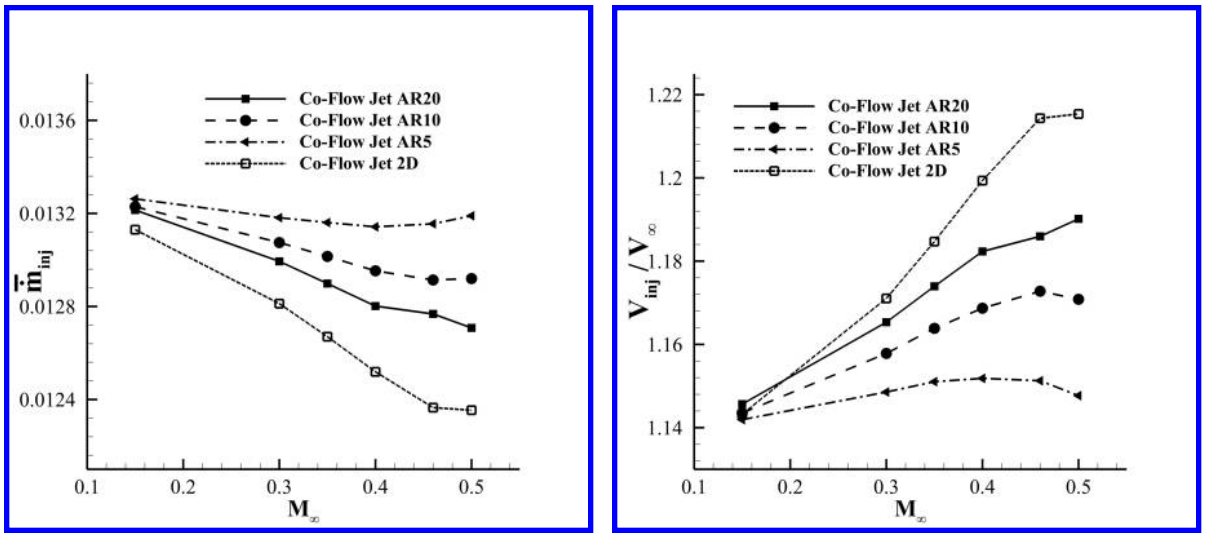


(a) (b)

Figure 9: Normalized mass flow rate and injection velocity plots for the 3D CFJ wings and 2D CFJ airfoil.



## 5 Analysis of 3D CFJ Wing Penalty

In order to understand the penalty of the 3D CFJ wing, the wing results are broken down to various components in Table. 8 and Table. 9 and are compared with the 2D results at Mach 0.30. Table. 9 lists the lift, drag, and moment coefficient and their detailed components from pressure, viscous force, and jet reactionary forces. As shown in Table. 8, the corrected aerodynamic efficiency $(C_L/C_D)_c$ drops substantially from 80.33 to 28.74 when the configuration is changed from 2D to 3D with $AR$ of 20.

Table 8: Performance at $M_\infty$ 0.30 for the 3D CFJ Wing with Different $AR$ and 2D CFJ airfoil.

| Dimension | AR | $AoA$ | $C_L/C_D$ | $(C_L/C_D)_c$ | $({C_L}^2/C_D)_c$ | $P_c$ | $PR$ | $P_{tinj}$ | $\dot{m}/Span$ | $V_{inj}$ |
|---|---|---|---|---|---|---|---|---|---|---|
| 2D | Infinity | 5° | 139.52 | 80.33 | 113.19 | 0.0074 | 1.0668 | 8.2025 | 0.0128 | 1.1710 |
| 3D | 20 | 5° | 36.56 | 28.74 | 35.55 | 0.0092 | 1.0737 | 8.3274 | 0.0130 | 1.1653 |
| 3D | 10 | 5° | 23.09 | 19.02 | 21.12 | 0.0103 | 1.0761 | 8.3940 | 0.0131 | 1.1578 |
| 3D | 5 | 5° | 14.67 | 12.39 | 11.46 | 0.0116 | 1.0786 | 8.4782 | 0.0132 | 1.1486 |

Based on Table. 8 and Table. 9, the factors decreasing the $(C_L/C_D)_c$ of the $AR$ 20 CFJ wing compared with the 2D airfoil include: 1) the lift coefficient drops by 12%; 2) the total drag coefficient is increased by 240% from 0.01 to 0.034, which is mostly due to the increased induced drag.; 3) the power coefficient $Pc$ is increased by 24% from 0.0074 to 0.0092.

Among the drag contributions, the majority of the drag increase is due to the pressure drag increase, which is determined by the induced drag. The friction drag is only increased by 7.6%. The CFJ reactionary force generates about the same thrust for the 2D and 3D cases at the thrust coefficient level of -0.095. The CFJ also reduce the total lift by the same amount between the 2D and 3D at the lift coefficient level of -0.54.

Table 9: Detailed lift contribution at $M_\infty$ 0.30 for the 3D CFJ wing at Different $AR$ and 2D CFJ airfoil.

| Dimension | AR | $AoA$ | $C_L$ | $C_D$ | $C_M$ | $C_{LP}$ | $C_{LV}$ | $C_{DP}$ | $C_{DV}$ | $F_x$ | $F_y$ |
|---|---|---|---|---|---|---|---|---|---|---|---|
| 2D | N/A | 5° | 1.409 | 0.010 | -0.179 | 1.944 | 0.000374 | 0.097 | 0.00758 | -0.094 | -0.535 |
| 3D | 20 | 5° | 1.237 | 0.034 | -0.173 | 1.779 | 0.000630 | 0.120 | 0.00816 | -0.095 | -0.542 |
| 3D | 10 | 5° | 1.110 | 0.048 | -0.169 | 1.657 | -0.000101 | 0.135 | 0.00853 | -0.095 | -0.546 |
| 3D | 5 | 5° | 0.925 | 0.063 | -0.160 | 1.477 | -0.000311 | 0.149 | 0.00895 | -0.095 | -0.552 |

Fig. 10 shows the Mach contour for 2D CFJ airfoil at at $M_\infty$ 0.30 and $AoA$ of 5°. Fig. 11 and Fig. 12 show the Mach contours for 3D CFJ and Baseline wings at $M_\infty$ 0.30 and $AoA$ of 5°. As we can see, the 2D airfoil Mach contour has the highest Mach number 0.558, whereas it is 0.537 for the CFJ wing at $AR$ 20 and 0.515 for the baseline wing at $AR$ 20. The maximum Mach number decreases with the decrease of aspect ratio. Also, the high velocity region near the injection slot on the suction surface is increased with the increase of the span location toward the wing tip.

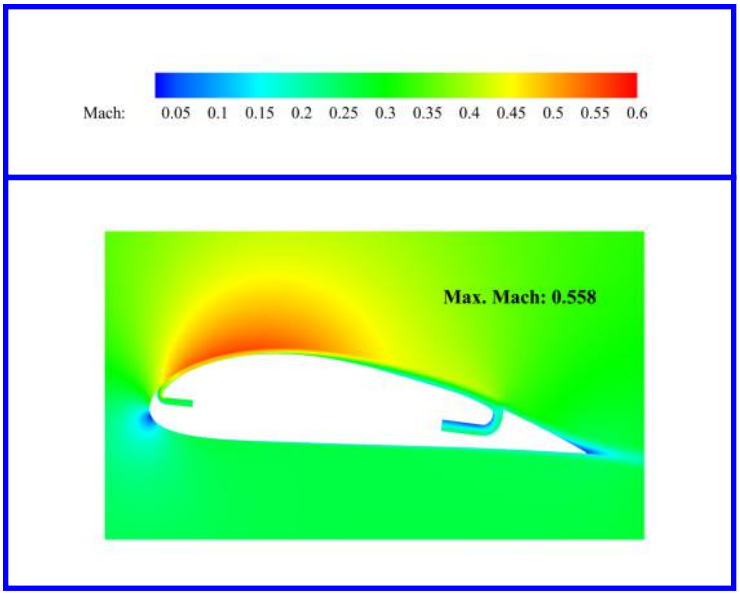


Figure 10: Mach contour for 2D CFJ airfoil at $M_\infty$ 0.30 and $AoA$ of 5°.

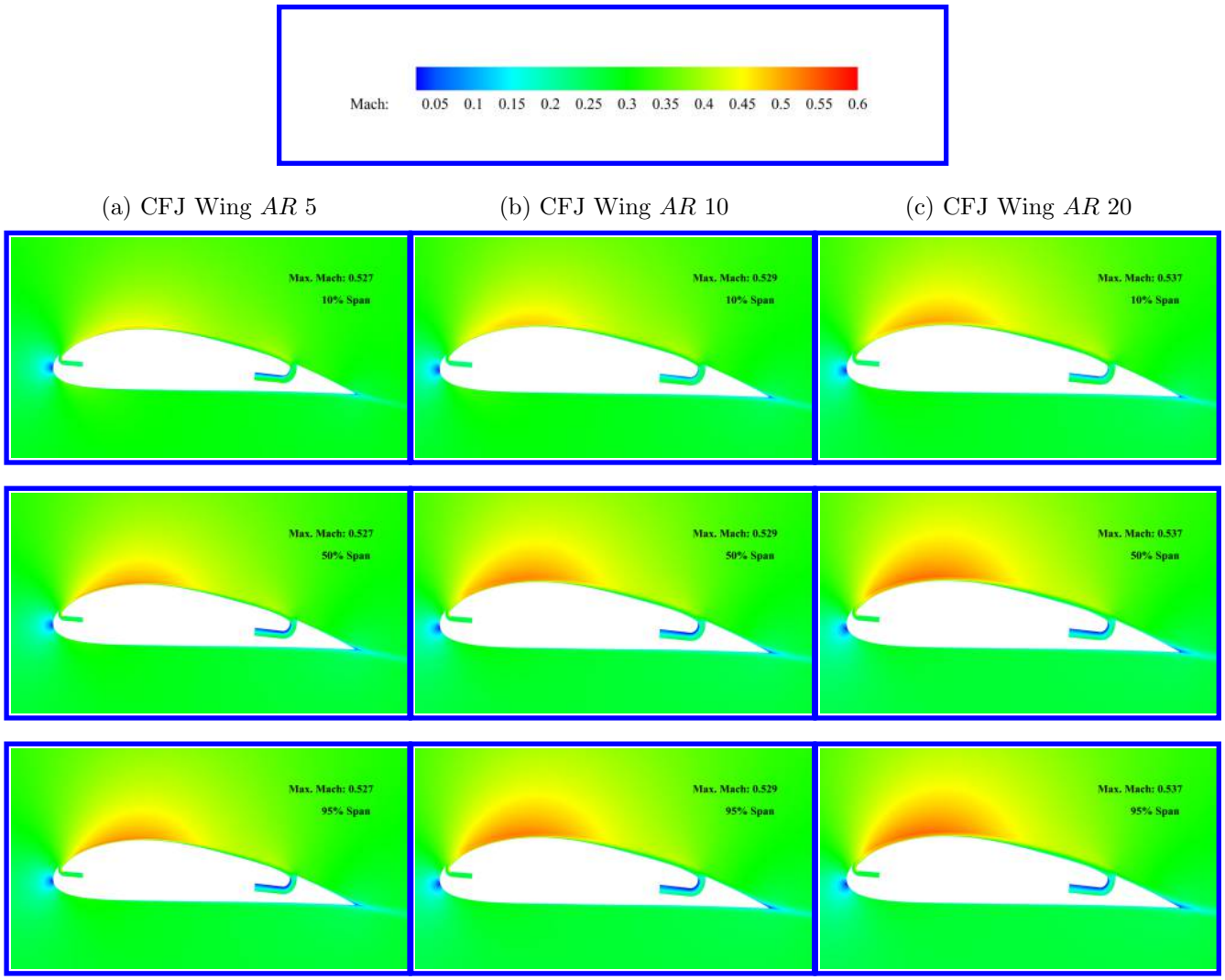


Figure 11: Mach contours at 10%, 50% and 95% spanwise location for the CFJ wing at different $AR$, $AoA = 5°$, $M_\infty = 0.30$.

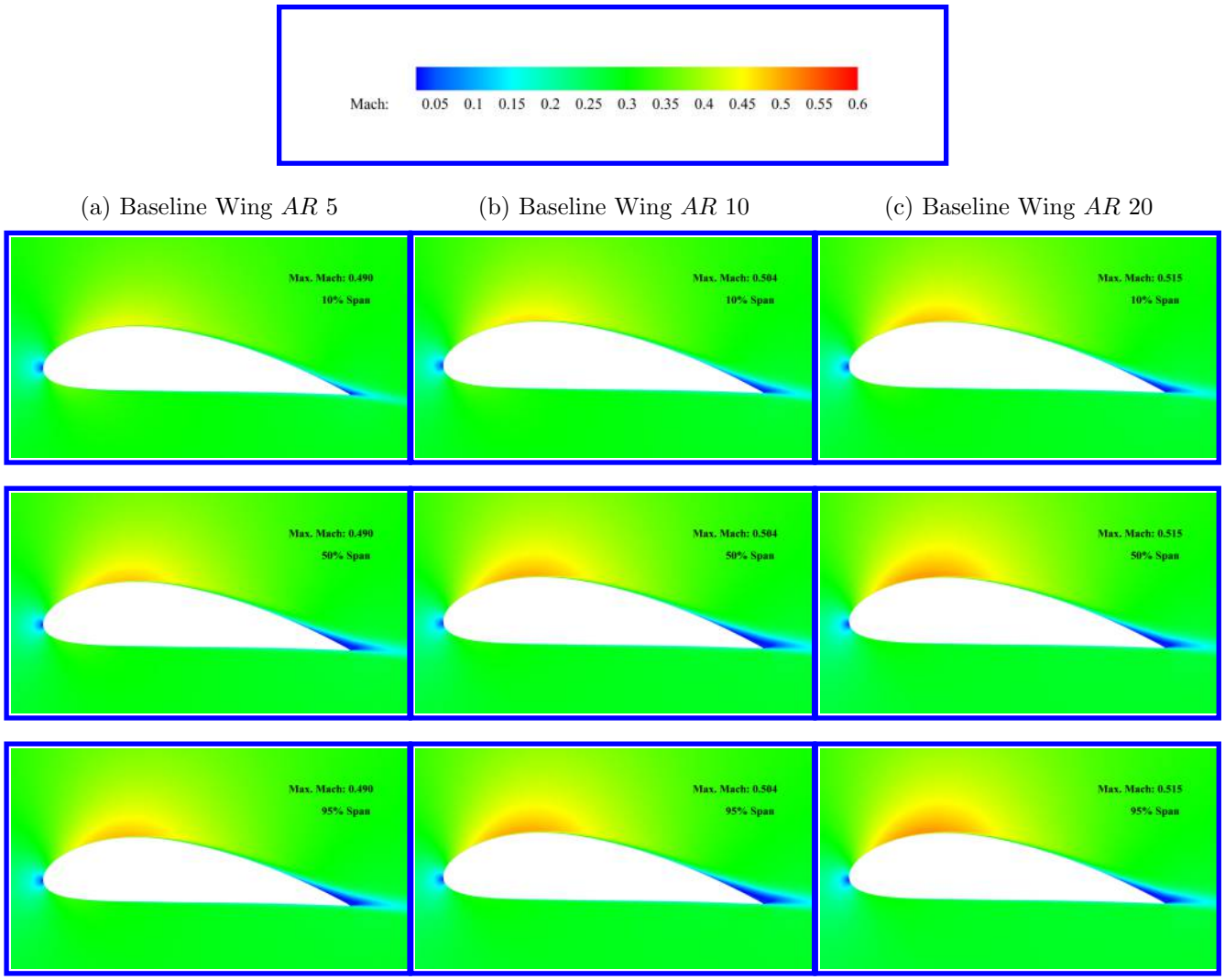


(a) Baseline Wing $AR$ 5 (b) Baseline Wing $AR$ 10 (c) Baseline Wing $AR$ 20

Figure 12: Mach contours at 10%, 50% and 95% spanwise location for baseline wing at different $AR$, $AoA = 5°$, $M_\infty = 0.30$.

Fig. 13 shows the CFJ wing surface static pressure contours at $M_\infty$ of 0.30 with the streamlines showing tip vortex colored with the vorticity at $AR$ 20, 10, and 5. They are plotted with the same scale for comparison. As we can see, the tip vortex is stronger at the wing tip with lower aspect ratio.

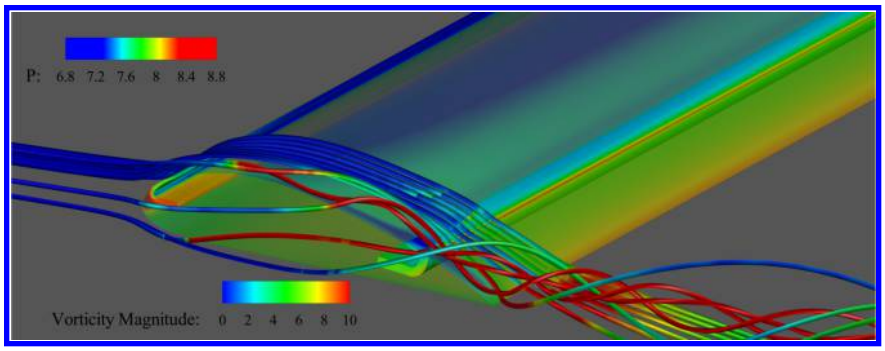


(a) 3D CFJ Wing at $AR$ 20 and $C_\mu$ 0.03

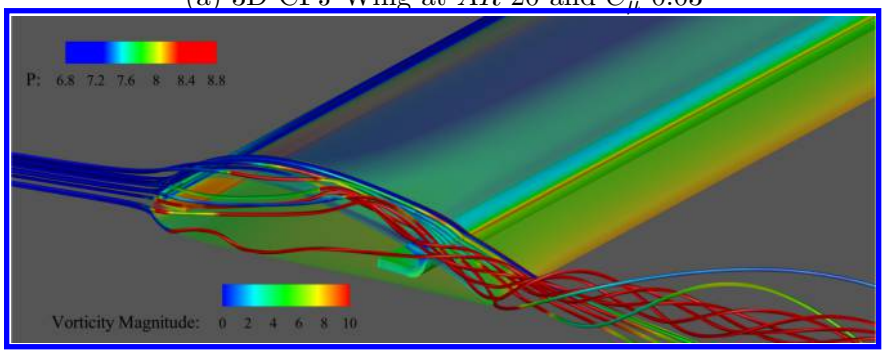


(b) 3D CFJ Wing at $AR$ 10 and $C_\mu$ 0.03

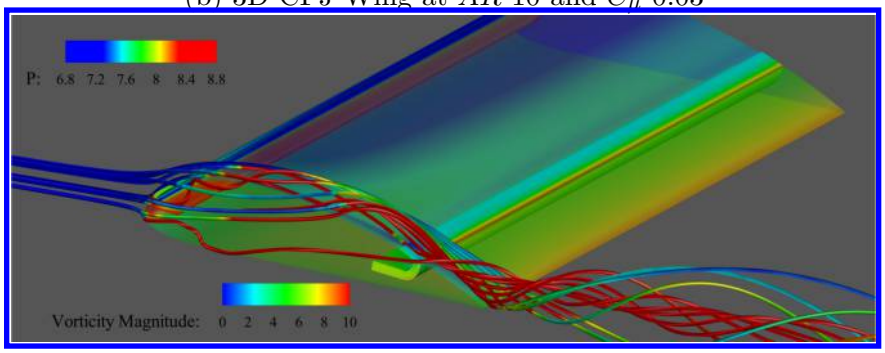


(c) 3D CFJ Wing at $AR$ 5 and $C_\mu$ 0.03

Figure 13: Tip vortex shown at pressure distribution and the tip vorticity magnitude plot of the 3D CFJ wing of aspect ratio 20, 10, 5 at $AoA$ of 5°.



## 6 Conclusion

This paper numerically studies the Mach number effect on cruise performance of 3D Co-Flow Jet (CFJ) wings at freestream Mach number of 0.15, 0.30, 0.35, 0.40, 0.46 and 0.50. The non-swept wing with three aspect ratios ($AR$) of 5, 10 and 20 based on CFJ-NACA-6421 airfoil are investigated. The numerical simulations employ the intensively validated in house FASIP CFD code, which utilizes a 3D RANS solver with Spalart-Allmaras (S-A) turbulence model, 3rd order WENO scheme for the inviscid fluxes, and 2nd order central differencing for the viscous terms. Similar to the previous 2D study, the 3D lift coefficient is increased with the Mach number due to compressibility effect. However, the overall aerodynamic efficiency and productivity are substantially dropped from 2D to 3D due to increased induced drag and the CFJ power coefficient. The penalty is further increased with the decreased aspect ratio. Compared with the baseline 3D wing with NACA-6421 airfoil at the same aspect

ratio, the cruise lift coefficient is increased on the average by about 30% for $AR$ of 5 and 60% for $AR$ of 20. For the $AR$ of 20, the pure aerodynamic lift to drag ratio $C_L/C_D$ is also increased by about 30%. Considering the CFJ pumping power consumption, the equivalent aerodynamic efficiency $(C_L/C_D)_c$ is about the same as the baseline wing. The productivity efficiency $(C_L^2/C_D)_c$ are increased by about 30% due to the increased lift coefficient. For $AR$ of 5, no efficiency advantage is obtained even though the high cruise lift coefficient remains. One important advantage for the CFJ active flow control is that it can use thick airfoil such as the 21% thickness for the whole flight envelop since CFJ airfoil has high resistance for flow separation. Thick airfoil can provide high lift coefficient and lighter structure weight. As an example shown in this study for cruise Mach number of 0.5, the wing with $AR$ of 20 has a cruise lift coefficient of 1.45, which is far greater than the lift coefficient of 0.5 - 0.7 for conventional subsonic wings. The advantage of a thick CFJ airfoil is that it provides high lift coefficient for the whole flight envelop and reduces the structure weight.



## 7 Acknowledgment

The simulations are conducted on Pegasus super computing system at the Center for Computational Sciences at the University of Miami.

Disclosure: Dr. GeCheng Zha is on the Board of Directors/Corporate Officer for CoFlow Jet and holds equity in CoFlow Jet. Dr. Zha is also the inventor of intellectual property licensed to CoFlow Jet.

## References

[1] G.-C. Zha and D. C. Paxton, "A Novel Flow Control Method for Airfoil Performance Enhancement Using Co-Flow Jet." *Applications of Circulation Control Technologies*, Chapter 10, p. 293-314, Vol. 214, Progress in Astronautics and Aeronautics, AIAA Book Series, Editors: Joslin, R. D. and Jones, G.S., 2006.

[2] G.-C. Zha, W. Gao, and C. Paxton, "Jet Effects on Co-Flow Jet Airfoil Performance," *AIAA Journal, No. 6,*, vol. 45, pp. 1222–1231, 2007.

[3] G.-C. Zha, C. Paxton, A. Conley, A. Wells, and B. Carroll, "Effect of Injection Slot Size on High Performance Co-Flow Jet Airfoil," *AIAA Journal of Aircraft*, vol. 43, 2006.

[4] G.-C. Zha, B. Carroll, C. Paxton, A. Conley, and A. Wells, "High Performance Airfoil with Co-Flow Jet Flow Control," *AIAA Journal*, vol. 45, 2007.

[5] Wang, B.-Y. and Haddoukessouni, B. and Levy, J. and Zha, G.-C., "Numerical Investigations of Injection Slot Size Effect on the Performance of Co-Flow Jet Airfoil," *Journal of Aircraft*, vol. Vol. 45, No. 6,, pp. pp.2084–2091, 2008.

[6] B. P. E. Dano, D. Kirk, and G.-C. Zha, "Experimental Investigation of Jet Mixing Mechanism of Co- Flow Jet Airfoil." AIAA-2010-4421, 5th AIAA Flow Control Conference, Chicago, IL, 28 Jun - 1 Jul 2010.

[7] B. P. E. Dano, G.-C. Zha, and M. Castillo, "Experimental Study of Co-Flow Jet Airfoil Performance Enhancement Using Micro Discreet Jets." AIAA Paper 2011-0941, 49th AIAA Aerospace Sciences Meeting, Orlando, FL, 4-7 January 2011.

[8] A. Lefebvre, B. Dano, W. Bartow, M. Fronzo, and G. Zha, "Performance and energy expenditure of coflow jet airfoil with variation of mach number," *Journal of Aircraft*, vol. 53, no. 6, pp. 1757–1767, 2016.

[9] A. Lefebvre, G-C. Zha, "Numerical Simulation of Pitching Airfoil Performance Enhancement Using Co-Flow Jet Flow Control," *AIAA paper 2013-2517*, June 2013.

[10] A. Lefebvre, G-C. Zha, "Cow-Flow Jet Airfoil Trade Study Part I : Energy Consumption and Aerodynamic Performance," *32nd AIAA Applied Aerodynamics Conference, AIAA AVIATION Forum, AIAA 2014-2682*, June 2014.

[11] A. Lefebvre, G-C. Zha, "Cow-Flow Jet Airfoil Trade Study Part II : Moment and Drag," *32nd AIAA Applied Aerodynamics Conference, AIAA AVIATION Forum, AIAA 2014-2683*, June 2014.

[12] Lefebvre, A. and Zha, G.-C., "Trade Study of 3D Co-Flow Jet Wing for Cruise Performance." AIAA Paper 2016-0570, AIAA SCITECH2016, AIAA Aerospace Science Meeting, San Diego, CA, 4-8 January 2016.

[13] Lefebvre, A. and Zha, G.-C. , "Design of High Wing Loading Compact Electric Airplane Utilizing Co-Flow Jet Flow Control." AIAA Paper 2015-0772, AIAA SciTech2015: 53nd Aerospace Sciences Meeting, Kissimmee, FL, 5-9 Jan 2015.

[14] Wang, Yang and Zha, G.-C., "Study of Mach Number Effect for 2D Co-flow Jet Airfoil at Cruise Conditions." AIAA AVIATION Forum 2019, AIAA Aviation and Aeronautics Forum and Exposition, Dallas, Texas, June 17-21, 2019.

[15] Wang, Yang and Zha, G.-C., "Study of 3D Co-Flow Jet Wing Induced Drag and Power Consumption at Cruise Conditions." AIAA Paper 2019-0034, AIAA Scitech Forum 2019, San Diego, California, January 7-11, 2019.

[16] Yunchao Yang and Gecheng Zha, "Super-Lift Coefficient of Active Flow Control Airfoil: What is the Limit?." AIAA Paper 2017-1693, AIAA SCITECH2017, 55th AIAA Aerospace Science Meeting, Grapevine, January 9-13 2017.

[17] Lefebvre, A. and Dano, B. and Bartow, W. and Di Franzo, M. and Zha, G.-C., "Performance Enhancement and Energy Expenditure of Co-Flow Jet Airfoil with Variation of Mach Number." AIAA Paper 2013-0490, AIAA Journal of Aircraft, DOI: 10.2514/1.C033113, 2016.

[18] P. R. Spalart and S. R. Allmaras, "A one-equation turbulence model for aerodynamic flows," in *30th Aerospace Sciences Meeting and Exhibit, Aerospace Sciences Meetings, Reno, NV, USA, AIAA Paper 92-0439*, 1992.

[19] Y.-Q. Shen and G.-C. Zha, "Large Eddy Simulation Using a New Set of Sixth Order Schemes for Compressible Viscous Terms ," *Journal of Computational Physics*, vol. 229, pp. 8296–8312, 2010.

[20] Zha, G.C., Shen, Y.Q. and Wang, B.Y., "An improved low diffusion E-CUSP upwind scheme ," *Journal of Computer and Fluids*, vol. 48, pp. 214–220, Sep. 2011.

[21] Y.-Q. Shen and G.-Z. Zha , "Generalized finite compact difference scheme for shock/complex flowfield interaction," *Journal of Computational Physics*, vol. doi:10.1016/j.jcp.2011.01.039, 2011.

[22] Shen, Y.-Q. and Zha, G.-C. and Wang, B.-Y., " Improvement of Stability and Accuracy of Implicit WENO Scheme," *AIAA Journal*, vol. 47, No. 2, pp. 331–344, 2009.

[23] Shen, Y.-Q. and Zha, G.-C. and Chen, X.-Y., " High Order Conservative Differencing for Viscous Terms and the Application to Vortex-Induced Vibration Flows," *Journal of Computational Physics*, vol. 228(2), pp. 8283–8300, 2009.

[24] Shen, Y.-Q. and Zha, G.-C. , " Improvement of the WENO Scheme Smoothness Estimator," *International Journal for Numerical Methods in Fluids*, vol. DOI:10.1002/fld.2186, 2009.

[25] G.-C. Zha and E. Bilgen, "Numerical Study of Three-Dimensional Transonic Flows Using Unfactored Upwind-Relaxation Sweeping Algorithm," *Journal of Computational Physics*, vol. 125, pp. 425–433, 1996.

[26] B.-Y. Wang and G.-C. Zha, "A General Sub-Domain Boundary Mapping Procedure For Structured Grid CFD Parallel Computation," *AIAA Journal of Aerospace Computing, Information, and Communication*, vol. 5, No.11, pp. 2084–2091, 2008.

[27] Y.-Q. Shen, G.-C. Zha, and B.-Y. Wang, "Improvement of Stability and Accuracy of Implicit WENO Scheme ," *AIAA Journal*, vol. 47, pp. 331–344, 2009.